Inverted perovskite solar cells with transparent hole transporting layer based on semiconducting nickel oxide

Diego Di Girolamo, Fabio Matteocci, Enrico Lamanna, Emanuele Calabrò, Aldo Di Carlo, and Danilo Dini

Citation: AIP Conference Proceedings **1990**, 020011 (2018); doi: 10.1063/1.5047765
View online: https://doi.org/10.1063/1.5047765
View Table of Contents: http://aip.scitation.org/toc/apc/1990/1
Published by the American Institute of Physics

Inverted Perovskite Solar Cells with Transparent Hole Transporting Layer Based on Semiconducting Nickel Oxide

Diego Di Girolamo[1], Fabio Matteocci[2], Enrico Lamanna[2], Emanuele Calabrò[2], Aldo Di Carlo[2,3], Danilo Dini[1,a]

[1] *Dept. of Chemistry, University of Rome Sapienza, P.le A. Moro 5, 00185 Rome,Italy*
[2] *Centre for Hybrid and Organic Solar Energy (CHOSE), Dept. of Electronic Engineering, University of Rome Tor Vergata, Via del Politecnico 1, 00133 Rome, Italy*
[3] *Department of Semiconductor Electronics and Device Physics, National University of Science and Technology,Moscow 119049, Russia*

[a)]Corresponding author: danilo.dini@uniroma1.it

Abstract. Perovskite ($CH_3NH_3PbI_3$) solar cells (PSCs) were produced in the inverted architecture employing transparent nickel oxide (NiO) as hole transporting layer (HTL). The different functional layers of the photoconversion device were solution processed in ambient conditions the HTL of NiO being prepared via sol-gel and successively deposited by spin-coating. The conditions of preparation of the transparent HTL were optimized through the stabilization of the nickel-containing sol with bulky alcohols and strong inorganic acids. The photoactive layer of $CH_3NH_3PbI_3$ was deposited in air at high relative humidity (ca. 50-60%). The electron selective contact was constituted by spin coated 3′*H*-cyclopropa[1,9] [5,6]fullerene-C_{60}-I*h*-3′-butanoic acid 3′-phenyl methyl ester (PCBM) with solution processed 2,9-Dimethyl-4,7-diphenyl-1,10-phenanthroline (bathocuproine, BCP) as interlayer. The deposition of $CH_3NH_3PbI_3$ in ambient conditions as well as the processing of the BCP interlayer from solution simplified enormously the entire procedure of device fabrication. The largest value of photoconversion efficiency (PCE) we achieved with the inverted architecture photocells was 14 % with an average PCE of 12 %. The solar cells displayed an hysteresis-free behavior with excellent time stability of the maximum power output.

INTRODUCTION

In last few years the solar cell based on lead halide perovskites (APbX3 with A = monovalent cation and X= halide) as photoelectroactive materials has represented an extremely important breaktrough for the R&D community involved in photovoltaics [1]. This is justified by the excellent performances of conversion displayed by CH3NH3PbI3 (MAPI) based solar cells which reach nowadays PCE values of more than 20% [1-3]. PSCs consist in p-i-n [4] or n-i-p [2] junctions with a highly absorbing film of perovskite film (i) sandwiched between the electron- (n) and the hole- (p) selective contact. The most common architecture of PSCs is the n-i-p one which employs a transparent electron transporting layer (ETL). The n-i-p type represents the PSC configuration with the best performances reported insofar [3]. Nowadays, increasing attention is being directed towards the inverted architecture p-i-n, with the HTL on the transparent side of the device [4] for a variety of reasons: a) device's cost-effectiveness; b) high quality of the electronic properties of inorganic HTL/perovskite interface [5-8] ; c) suppression of hysteresis in the JV characteristic curves [9-11]. Inorganic materials as HTLs of inverted perovskite solar cells are interesting for their high temporal stability and peculiar optoelectronic properties [4-6]. For such a reason we directed our efforts in the analysis of a series of inverted PSCs that employed spin coated NiOx as inorganic HTL. The two main distinctive features of our device (Fig. 1) are related to the modality of fabrication: i) perovskite deposition in air; ii) solution processing of the BCP interlayer. The resulting PSCs showed PCE values as high as 13.7% with hysteresis-free JV curves and stable maximum power output.

NANOINNOVATION 2017
AIP Conf. Proc. 1990, 020011-1–020011-7; https://doi.org/10.1063/1.5047765
Published by AIP Publishing. 978-0-7354-1706-9/$30.00

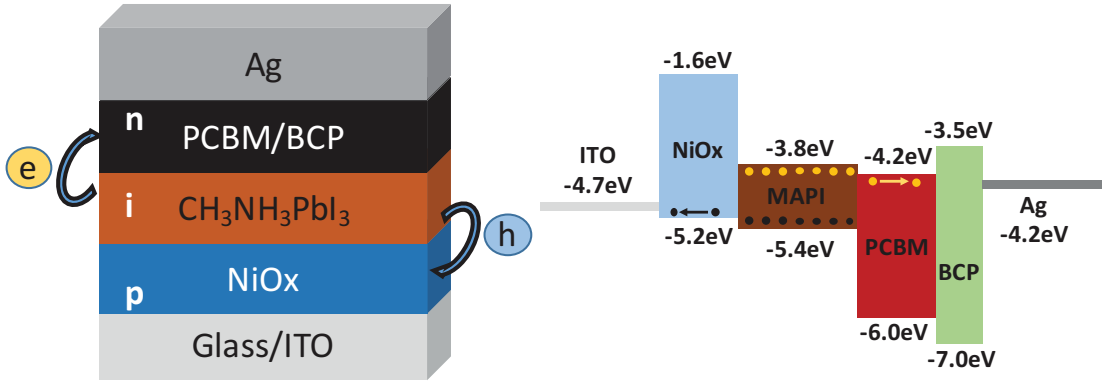

FIGURE 1. Left: Inverted architecture of the PSCs considered in this work. Right: scheme of the energy levels of the materials employed in device fabrication.

RESULTS AND DISCUSSION

When dealing with sol-gel chemistry of nickel oxide precursors an important issue is represented by the instability of the sol. According to literature, bulky alcohols are recommended to avoid precipitation of branched nickel alcoxides [11]. In fact, we observed quick precipitation when common alcoholic solvents like ethanol or iso-propanol were employed. The phenomenon of precipitation is relented, but not arrested, when alcohols of the *cellosolve* family, e.g. 2-methoxyethanol, are used. It has been observed that the presence of bulky 2-methoxyethanol in the sol does not improve the stability at room temperature. The precipitate can be dissolved again upon increase of temperature the extent of which depends on the concentration of the nickel precursor $Ni(acac)_2$ (=nickel acetylacetonate). The addition of typical chelating agents such us ethylene glycol or monoethanolamine even produced a more abrupt effect of precipitation with irreversible features. Acidic additives like HNO3 resulted successful for sol stabilization when the sol was composed by $Ni(acac)_2$ in 2-methoxyethanol. The sol resulted indefinitely stable at room temperature within a large range of $Ni(acac)_2$ concentration. The NiOx precursor sol was spin-coated on glass/ITO substrates at the spin rate of 4000 rpm for 30 seconds. The final step of annealing consisted in the treatment of the deposit at 300°C for 1 hour with the final attainment of the NiOx HTL in the configuration of thin film [12-20]. Uniform and morphologically flat films of NiOx have been obtained through spin coating of the nickel sol (Fig. 2), with evidence of a mosaic texture of the film. The RMS surface roughness of spin coated NiOx was below 2nm.

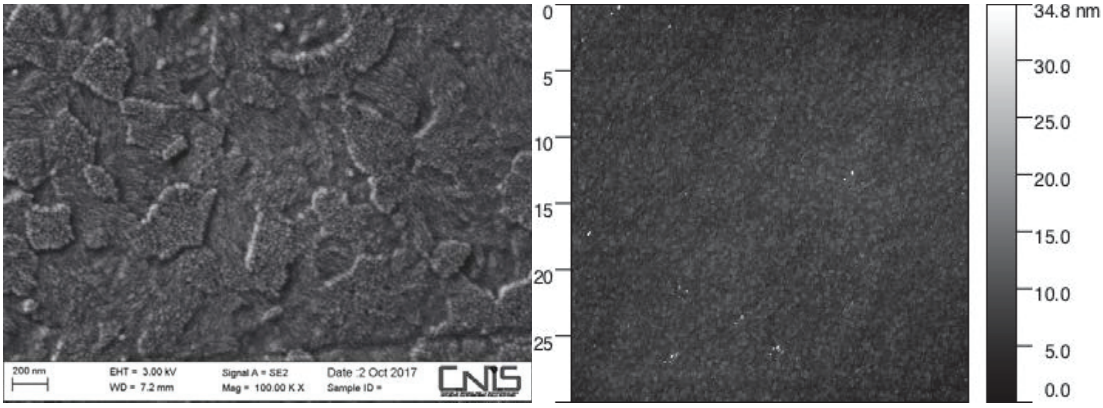

FIGURE 2. Morphological characterization of the NiO_x film obtained from a sol with 0.2M $Ni(acac)_2$. Left: SEM micrograph of NiO_x surface. Right: AFM topography.

NiO_x film showed an averaged transmittance of about 80% in the visible range. A continuous red shift of the glass/ITO interference pattern was observed upon increase of $Ni(acac)_2$ concentration in the sol. Such an effect would be the consequence of the modification of NiO_x film thickness [21] following the variation of precursor concentration.

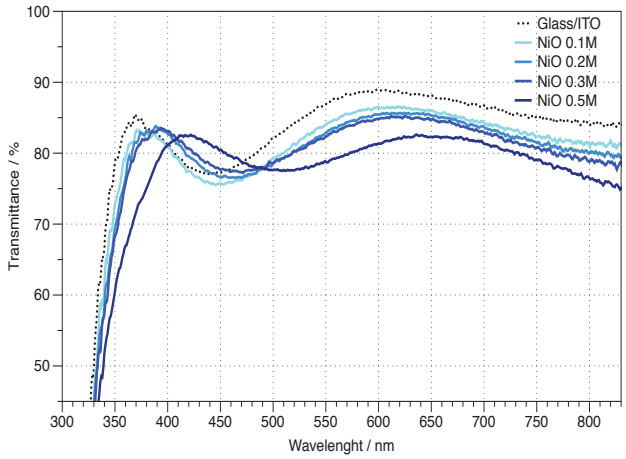

FIGURE 3. Transmittance spectra of different NiO_x thin films spin coated onto glass/ITO substrate.

The deposition of MAPI layer was conducted in air with relative humidity in the broad range 40-55%. MAPI deposition has been optimized employing a *solvent engineering* approach [22,23]. PbI_2 and MAI in the molar ratio 1:1 and at the concentration 1.41M were dissolved in DMF:DMSO (volume ratio: 9:1). Such a solution is spin coated on NiO_x substrate at 5000rpm with diethyl ether as *anti-solvent*. Thermal annealing in mild conditions at 50°C for 2 minutes and successively at 100°C for 10 minutes leads to the complete crystallization of MAPI. The optical spectrum of MAPI/NiO_x combination confirmed the successful cast of the $CH_3NH_3PbI_3$ layer onto the metal oxide (Fig. 4). The light-harvesting properties of the junction here reported in the 500-750nm spectral range are still inferior with respect to the systems that have produced more competitive values of PCEs [24]. Therefore, the aspect of MAPI loading onto sol-gel NiO_x substrates still requires further analysis. As proved with AFM (Fig. 2) NiO_x is an extremely flat substrate that, as a such, could prevent the anchorage of large amounts of perovskite precursor(s). Thicker films of MAPI are expected to be obtained by changing the deposition procedure (and eventually the roughness of the HTL), but this is not a trivial task and will be the object of further investigations.

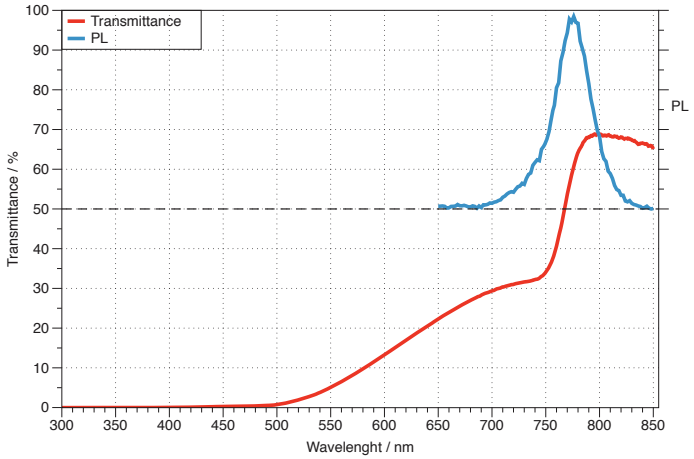

FIGURE 4. Red trace: optical transmission spectrum of the $CH_3NH_3PbI_3$ thin film deposited on glass/ITO/NiO_x substrate in ambient conditions. Blue trace: steady state photoluminescence spectrum of $CH_3NH_3PbI_3$ onto glass/ITO/NiO_x substrate.

The electron selective contact is obtained through the spin-coating deposition of PCBM from a 20mg/mL solution employing chlorobenzene as solvent. This step is followed by BCP spin coating from a 0.5mg/mL solution utilizing isopropanol as solvent. It is well known that PCBM/Ag interfaces have poor electrical properties with deleterious consequences on devices performances [25]. The electronic barrier to charge collection at the silver back contact of the PCBM/Ag interface could be lowered employing lower work function metals like Ca or Al or, alternatively, by inserting a suitable interlayer between PCBM and Ag [26]. In

particular, it has been found that electron collection is improved when a thin film of BCP (thickness: 5-10 nm) is interposed, usually through thermal evaporation, between PCBM and Ag layers [27,28]. Herein we successfully exploit the solution processing of the BCP interlayer for an inverted PSC similarly to what was reported in previous works on inverted PSCs with organic HTL [28]. The overall device fabrication procedure here considered results to be extremely simplified since the $CH_3NH_3PbI_3$ film is casted in air and the BCP interlayer deposited from solution.

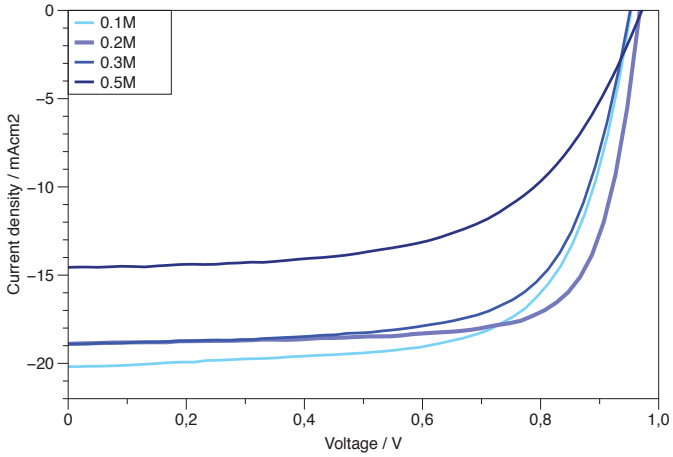

FIGURE 5. Characteristic curves of the best performing PSCs with NiO_x HTLs differing for the concentration of the Ni(acac) precursor in the sol.

TABLE 1. Characteristic parameters of the best performing PSCs presented in Figure 5. In round brackets the average values of the various parameters are reported.

$[Ni(acac)_2]$ / M	**V_{oc} / V**	**J_{sc} /mAcm^2**	**FF**	**PCE / %**
0.1	0.95 (0.930)	-20.18 (-19.90)	67.9 (62.7)	13.08 (11.64)
0.2	0.96 (0.960)	-18.90 (-18.58)	75.0 (65.9)	13.71 (11.78)
0.3	0.95 (0.951)	-18.89 (-18.20)	68.6 (65.6)	12.34 (11.35)
0.5	0.97 (0.910)	-14.40 (-14.67)	59.8 (52.2)	8.39 (7.02)

Figure 5 reports the JV curves of the best performing PSCs with NiO_x HTLs that differed for the concentration of the nickel salt in the precursor sol (range 0.1- 0.5 M). The analysis of the photovoltaic performance of the different devices (Table 1) shows that there is an optimum value of precursor concentration for the individuation of the most efficient PSC: when $[Ni(acac)_2]$ = 0.2 M the corresponding cell has a PCE reaching a maximum of 13.7 % and a maximum of fill factor (FF) of 75%. On the other hand, no trend for the open circuit voltage V_{oc} could be observed upon variation of precursor concentration (Table 1). A plausible explanation for that is due to the recognition that the quality of the MAPI/ETL interface represents the actual limiting factor for the parameter of V_{oc}. Several works have reported on the negative influence of PCBM on V_{oc} due to energetic disorder as well as poor electronic transport [29]. Our supposition is also in accord with the observation of a clear effect of light soaking which mainly affects the transport properties through the $CH_3NH_3PbI_3$/PCBM interface: V_{oc} increases of about 150 mV starting from an initial value of ca. 800 mV after 2 minutes of illumination [30,31]. The short circuit photocurrent density, J_{SC}, generally decreases upon increase of the precursor concentration, with the largest diminution of J_{SC} in passing from 0.3 to 0.5 M (Table 1). From the analysis of the results summarized in Table 1 it is recognized that the NiO_x-HTL processed from the 0.2 M sol shows the higher values of PCE and FF due to a good tradeoff between series and shunt resistance of the devices. From the slope close to V_{OC} of the JV profiles is possible to guess a low series resistance for all devices except the one derived from the 0.5 M sol. As far as the shunt resistance is concerned the relatively lower value of this electrical parameter is observed with the 0.1 M device due to the observation of a slope in the JV curve close to short circuit condition. At a physical level it is presumed that for the 0.2 M device an optimum tradeoff between uniform coverage of the substrate and homogeneity of the NiO_x compact layer is achieved. The

uniform coverage of the substrate would prevent the formation of electrical paths of lower resistance (shunt effects), whereas a homogeneous thin layer of HTL accompanies a generally low series resistance. The top value of PCE=13.7% is certainly a very promising result and a considerable achievement for a NiO_x based inverted PSC when the photoactive layer of perovskite is deposited in ambient conditions.

The statistical analysis realized on a set of 10 nominally equal devices for each type of PSC is reported in Fig. 6. The small amplitudes of the intervals of variation for the four different photovoltaic parameters indicates the good reproducibility of the method of fabrication here adopted.

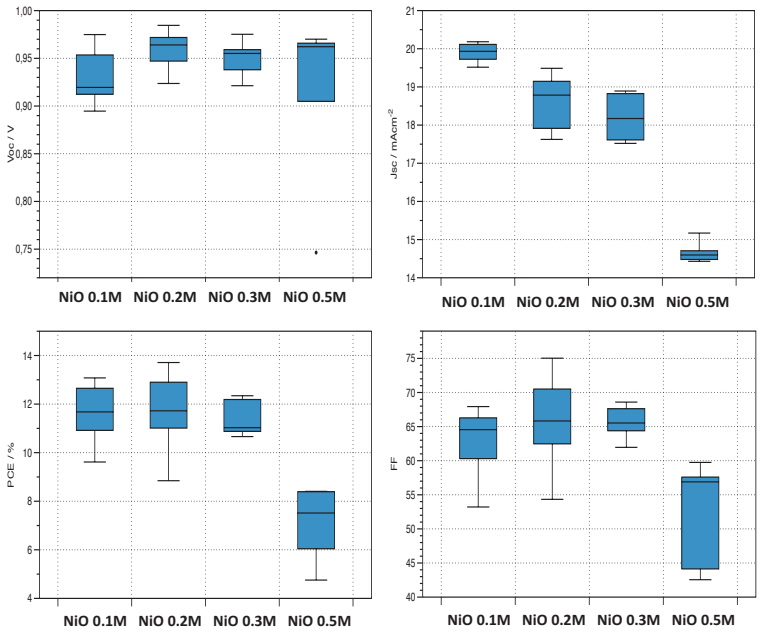

FIGURE 6. Statistics of the four main photovoltaic parameters for the PSCs differing in the type of NiO_x-HTL.

Our devices did not show evidences of hysteresis phenomena (Fig. 7, left frame) as evidenced from the complete overlap of the profiles obtained during the direct and reverse scans. For the various devices under examination the time-variations of the characteristics of maximum power (MP) point were also recorded (Fig. 7, right frame). The normalized values of V_{MP}, J_{MP} and P_{MAX} displayed unit value during the firsts two minutes of observation, thus confirming the significance of MP obtained from J-V curves.

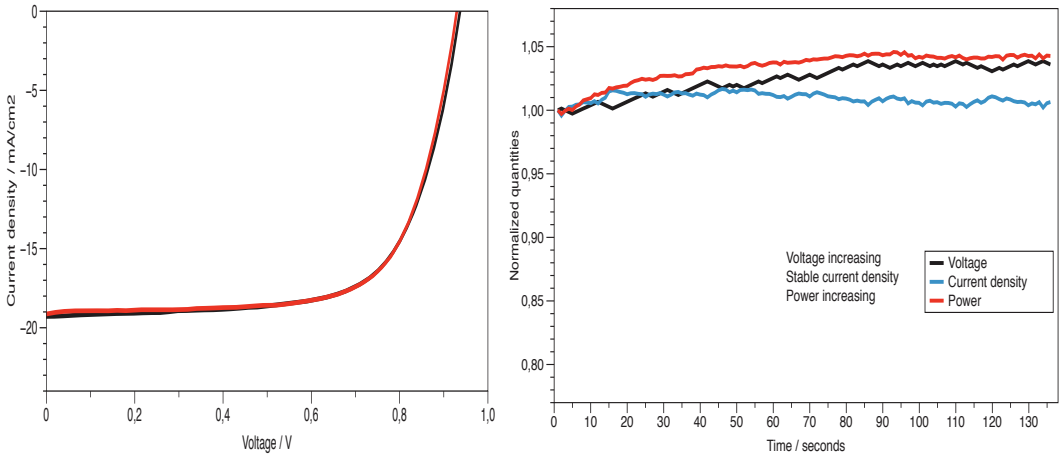

FIGURE 7. Left: contours of the JV profiles during the direct (black trace) and reverse (red trace) scan. Right: normalized time-variations of voltage, current density and power output for a representative device in correspondence of the point of maximum power.

CONCLUSIONS

We reported a reproducible procedure of inverted PSCs fabrication with attainment of ca. 14% as maximum PCE when sol-gel NiO_x was the HTL. This represents a remarkable result considering that $CH_3NH_3PbI_3$ is deposited in ambient conditions. The conditions of spin coating deposition of the NiO_x HTL prepared via sol-gel have been optimized and an improvement of nickel sol stability was achieved. The performances of the NiO_x-derived PSCs have been analyzed and compared to the results recently reported in literature for devices with similar configuration. It is believed that this series of results represents a promising starting point for further optimization of the PSCs with NiO_x HTL especially with regard to the introduction of doping strategies for improvement of NiO_x electrical properties and with regard to the targeted optimization of the $CH_3NH_3PbI_3$/PCBM interface.

ACKNOWLEDGMENTS

The authors acknowledge the financial support from MIUR which funded the research project PRIN 2010–2011 (protocol no. 20104XET32). DD acknowledges the financial support from the University of Rome "LA SAPIENZA" through the program Ateneo 2016 (Protocol No. RM116154C3864CF2). ADC thanks Regione Lazio and CHOSE for the technical support of the research conducted at the University of Rome "TOR VERGATA". ADC gratefully acknowledges the financial support of the Ministry of Education and Science of the Russian Federation in the framework of Increase Competitiveness Program of NUST «MISiS» (No. K2-2017- 025), which has been implemented by the governmental decree N 211 dated 16th of March 2013.

REFERENCES

1. Correa-Baena, J.P.; Abate, A.; Saliba, M.; Tress, W.; Jacobsson, T. J.; Graetzel, M. G. X.; Hagfeldt, A. Energy Environ. Sci. **10**, 710–727, (2017).
2. Yang, W. S., Park, B. W., Jung, E. H., Jeon, N. J., Kim, Y. C., Lee, D. U., ... & Seok, S. I. Science **356(6345)**,1376-1379 , (2017).
3. NREL Best Research Cell Efficiency Chart.
4. Liu, T., Chen, K., Hu, Q., Zhu, R., & Gong, Q. ,Advanced Energy Materials **6(17)**, (2016).
5. Li, M. H., Yum, J. H., Moon, S. J., & Chen, P. ,Energies **9(5)**, 331, (2016).
6. Li, M. H., Shen, P. S., Wang, K. C., Guo, T. F., & Chen, P. Journal of Materials Chemistry A **3(17)**, 9011-9019,(2015).
7. Yu, Z., & Sun, L. , Small Methods **2**, 1700280 (2018).
8. Arora, N., Dar, M. I., Hinderhofer, A., Pellet, N., Schreiber, F., Zakeeruddin, S. M., & Grätzel, M. Science **eaam5655**, (2017).
9. Xu, J., Buin, A., Ip, A. H., Li, W., Voznyy, O., Comin, R., ... & Kanjanaboos, P. Nature communications **6**, (2015).
10. Shao, Y., Xiao, Z., Bi, C., Yuan, Y., & Huang, J. Nature communications **5**, 5784, (2014).
11. Livage, J., & Ganguli, D. Solar Energy Materials and Solar Cells **68(3)**, 365-381, (2001).
12. Dini, D., Halpin, Y., Vos, J. G., & Gibson, E. A. Coordination Chemistry Reviews **304**, 179-201, (2015).
13. Awais, M., Rahman, M., MacElroy, J. D., Coburn, N., Dini, D., Vos, J. G., & Dowling, D. P. Surface and Coatings Technology **204(16)**, 2729-2736, (2010).
14. Awais, M., Rahman, M., MacElroy, J. D., Dini, D., Vos, J. G., & Dowling, D. P. Surface and Coatings Technology **205**, S245-S249, (2011).
15. Awais, M., Dowling, D. D., Rahman, M., Vos, J. G., Decker, F., & Dini, D. Journal of Applied Electrochemistry **43(2)**, 191-197, (2013).
16. Gibson, E. A., Awais, M., Dini, D., Dowling, D. P., Pryce, M. T., Vos, J. G., ... & Hagfeldt, A. Physical Chemistry Chemical Physics **15(7)**, 2411-2420, (2013).
17. Awais, M., Dini, D., MacElroy, J. D., Halpin, Y., Vos, J. G., & Dowling, D. P. Journal of Electroanalytical Chemistry **689**, 185-192, (2013).
18. Awais, M., Gibson, E., Vos, J. G., Dowling, D. P., Hagfeldt, A., & Dini, D. ChemElectroChem **1(2)**, 384-391, (2014).
19. Awais, M., Dowling, D. P., Decker, F., & Dini, D. Advances in Condensed Matter Physics **2015**, 186375 (2015).
20. Awais, M., Dowling, D. D., Decker, F., & Dini, D. SpringerPlus **4(1)**, 564, (2015).
21. Dini, D., Decker, F., & Masetti, E. Journal of applied electrochemistry **26(6)**, 647-653, (1996).

22. Ahn, N., Son, D. Y., Jang, I. H., Kang, S. M., Choi, M., & Park, N. G. Journal of the American Chemical Society **137(27)**, 8696-8699, (2016).
23. Dagar, J., Castro-Hermosa, S., Gasbarri, M., Palma, A. L., Cina, L., Matteocci, F., ... & Brown, T. M. Nano Research, 1-13.Liu, J., Wang, G., Luo, K., He, X., Ye, Q., Liao, C., & Mei, J. ChemPhysChem **18(6)**, 617-625, (2017).
24. Jung, J. W., Chueh, C. C., & Jen, A. K. Y. Advanced Energy Materials **5(17)**, (2015).
25. Bai, Y., Meng, X., & Yang, S. Advanced Energy Materials **8**, 1701883, (2017).
26. Liu, J., Wang, G., Luo, K., He, X., Ye, Q., Liao, C., & Mei, J. ChemPhysChem **18(6)**, 617-625, (2017).
27. Jeng, J. Y., Chen, K. C., Chiang, T. Y., Lin, P. Y., Tsai, T. D., Chang, Y. C., ... & Hsu, Y. J. Advanced materials **26(24)**, 4107-4113, (2014).
28. Yuan, D. X., Yuan, X. D., Xu, Q. Y., Xu, M. F., Shi, X. B., Wang, Z. K., & Liao, L. S. Physical Chemistry Chemical Physics **17(40)**, 26653-26658, (2015).
29. Shao, Y., Yuan, Y., & Huang, J. Nature Energy **1(1)**, (2016).
30. Shao, S., Abdu-Aguye, M., Qiu, L., Lai, L. H., Liu, J., Adjokatse, S., ... & Kooi, B. J. Energy & Environmental Science **9(7)**, 2444-2452, (2016).
31. Zhang, T., Cheung, S. H., Meng, X., Zhu, L., Bai, Y., Ho, C. H. Y., ... & Yang, S. The Journal of Physical Chemistry Letters **8(20)**, 5069-5076, (2017).